第 32 卷第 12 期 无 机 化 学 学 报 Vol.32 No.12
2016 年 12 月 CHINESE JOURNAL OF INORGANIC CHEMISTRY 2172-2182

喹啉类单核锰(Ⅱ)和钴(Ⅱ)配合物的合成、结构、DNA/BSA 键合及 DNA 切割活性

张永坡 杨佳佳 吕佳苑 高春艳* 赵晋忠*
(山西农业大学文理学院,太谷 030801)

摘要:合成了 2 个结构类似的喹啉类单核锰和钴配合物[$ML(H_2O)_3$]·H_2O,其中 M 为 Mn (**1**)、Co (**2**),Na_2L 为 8-(羧基钠甲氧基)喹啉-2-甲酸钠。运用红外光谱、元素分析和 X 射线单晶衍射表征了其结构。利用电子吸收和发射光谱法研究了配合物与 CT-DNA 及 BSA 的键合作用及配合物对 DNA 的切割作用。晶体解析结果表明 2 个配合物为同构结构,配合物中心均为七配位的畸变五角双锥结构。钴配合物 **2** 与 CT-DNA 的键合能力强于锰配合物 **1**,两者与 BSA 的作用机理为静态淬灭机理,而键合常数值大小为 **1**>**2**。在以 H_2O_2 作为诱导剂时,在同等条件下,**2** 切割 DNA 的能力明显增强。通过加入自由基捕获剂证明了配合物对 DNA 的切割机理为氧化切割机理,其中活性氧为 OH·。

关键词:配合物;喹啉类配体;DNA/BSA 键合;DNA 切割
中图分类号:O614.71+1;O614.81+2 **文献标识码**:A **文章编号**:1001-4861(2016)12-2172-11
DOI:10.11862/CJIC.2016.265

Syntheses, Structures, DNA/BSA Binding and DNA Cleavage of Mononuclear Manganese(Ⅱ) and Cobalt(Ⅱ) Complexes with *N*,*O*-Chelating Quinoline Derivative Ligand

ZHANG Yong-Po YANG Jia-Jia LÜ Jia-Yuan GAO Chun-Yan* ZHAO Jin-Zhong*
(*College of Arts and Sciences, Shanxi Agricultural University, Taigu, Shanxi* 030801, *China*)

Abstract: Two new mononuclear complexes [$ML(H_2O)_3$]·H_2O (M=Mn (**1**) and Co (**2**)) of quinoline derivative ligand (Na_2L =sodium 8-(carboxylatomethoxy)quinoline-2-carboxylate) have been synthesized and characterized. The complexes are isostructural and both metal centers are heptacoordinated with O_6N donor sets and the geometry around metal centers can be best described as distorted pentagonal bipyramidal. Interactions of the complexes with CT-DNA and BSA have been explored by absorption and emission spectral methods. Binding abilities of the complexes to CT-DNA display a relative order: **2**>**1**, while the quenching mechanisms of BSA by both complexes are static procedures and the binding constant values follow the order: **1**>**2**. In the presence of H_2O_2 as a revulsant or an activator, compared with complex **1**, the DNA cleavage efficiency of **2** exhibited more remarkable increases at the same conditions. Oxidative mechanism has been demonstrated by adding standard radical scavengers and the reactive oxygen species (ROS) responsible for the DNA cleavage is likely hydroxyl radicals (OH·). CCDC: 1040326, **1**; 1040325, **2**.

Keywords: complexes; quinoline ligand; DNA/BSA binding; DNA cleavage

收稿日期:2016-06-15。收修改稿日期:2016-09-29。
山西农业大学引进人才科研启动金(No.2013YJ40,2013YJ41)、山西农业大学科技创新基金(No.2014013,2014005)、山西农业大学大学生科技创新项目(No.13-017,2015085)、山西省高等学校大学生创新创业训练项目(No.2015085, 2015106)和山西省煤基重点项目(No.FT201402-01)资助。
*通信联系人。E-mail:gaocynk@163.com,zhaojinzhongnd@126.com;会员登记号:S06N2534M1605。

0 Introduction

Metal complexes are a significant class of compounds with biological activities that can be potentially used in gene regulation, probing of DNA specific structures and interactions, and design of therapeutic agents[1-3]. Since the discovery of antitumor activity of cisplatin in the 1960s[4-5], the research field of metal-based therapeutics has received considerable attention and broad interest[6-7]. Metal complexes have natural propensity to interact with DNA due to their cationic characteristic, and based on their wide spectrum of ligands and broad range of structural geometries[8] as well as kinetic properties and mechanisms of drug action[9].

It has been widely accepted that DNA is the primary biological targets of metal-based therapeutics in vivo[10]. Interactions of metal complexes with DNA range from electrostatic interaction to strong covalent bonding, DNA intercalation, groove binding, hydrogen-bonding with ligands, and cleavage of DNA[11-14]. Transition metal complexes as synthetic metallonucleases have been studied extensively due to their supporting a multitude of coordination numbers and geometries. Among them, application of cobalt and manganese are important because of their biologically relevant and lesser toxicity[15-16]. Mn and Co are widely distributed in natural nucleases. Several metalloenzymes in biosystem require Mn or Co as cofactor for their catalytic activities. This prompted us to study the DNA interaction as well as nuclease activity of Mn and Co complexes.

Apart from the choice of metal ion centers, purposeful design of these metal-based pharmaceuticals mainly depends on the various ligand frameworks. Structures and functionalities of ligands can significantly alter the biological properties by modifying the physical and chemical properties of the ion(s), including limiting the adverse effects of metal ion overload, inhibiting selected metalloenzymes, and facilitating metal ion redistribution[8]. Due to coplanar aromatic rings, quinoline is regarded as an efficient DNA intercalating group. 8-Hydroxylquinoline is a monoprotic bidentate chelating agent able to form a bis-substituted metal complex that inhibited proteasome activity, resulting in proliferation suppression and apoptosis induction in cultured breast and prostate cancer cells, showing potential anticancer activity[17-18].

Herein, we selected a typical 2-carboxyl and 8-oxo-ethyl acetate derived quinoline as ligand (Scheme 1). Similar hepta-coordinated Mn(Ⅱ) and Co(Ⅱ) compounds have been synthesized and characterized. In this paper an attempt has been made to investigate the effect of two different metal ions in the same ligand environment on the DNA/BSA binding ability of the complexes.

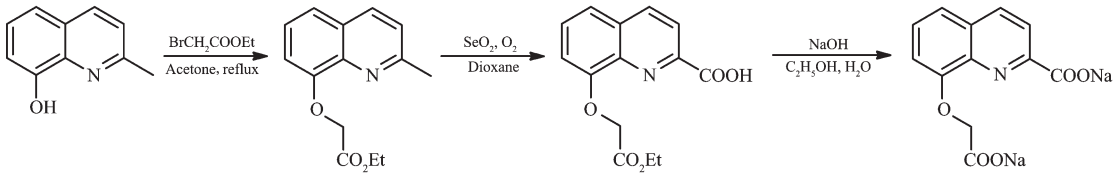

Scheme 1　Synthesis of Na_2L (sodium 8-(carboxylatomethoxy)quinoline-2-carboxylate)

1 Experimental

1.1 Materials and methods

All reagents and solvents were purchased from commercial sources and used without further purification. Plasmid pBR322 DNA, calf thymus (CT-DNA), bovine serum albumin (BSA) and ethidium bromide (EB) were purchased from Sigma-Aldrich. Stock solutions of Mn(Ⅱ) (1.0 mmol·L^{-1} in 32% DMF/H_2O) and Co(Ⅱ) (1.0 mmol·L^{-1} in 6% DMF/H_2O) complexes were stored at 4 ℃ and prepared to series concentrations for all experiments. Phosphate buffer and Tris-HCl solution were prepared using triple-distilled deionized sonicated water. Elemental analyses for C, H and N were performed on a Perkin-Elmer analyzer. IR spectra were obtained on a Perkin-

Elmer FTIR spectrometer in the range of 4 000~400 cm^{-1}. Electronic spectra were measured on a JASCO V-570 spectrophotometer. Fluorescence spectral data were collected on a MPF-4 fluorescence spectrophotometer at room temperature. Gel Imaging and documentation DigiDoc-It System were assessed using Labworks Imaging and UVI (England) Analysis Software.

1.2 Preparation of compounds

1.2.1 Synthesis of the ligand Na_2L

Ligand Na_2L was prepared using a similar method of the literature[19]. A mixture of 8-hydroxy-2-methylquinoline (2.4 g, 15 mmol), ethyl bromoacetate (2.5 g, 15 mmol) and powdered K_2CO_3 (8 g, 58 mmol) in acetone (30 mL) was refluxed for 24h. After cooled to room temperature, the mixture was centrifuged and filtered. The filtrate was evaporated to generate crude oil residue, which was redissolved in 25 mL of dioxane. 1.8 g SeO_2 (16 mmol) was added and the mixture was refluxed under an open air for 10 h. After cooled, the solvent was removed under vacuum. 50 mL 0.5 mol·L^{-1} HCl was added and the mixture was extracted by ethyl acetate. The organic phase was combined and concentrated to generate crude oil residue. The residue was redissolved in 25 mL of ethanol, and a solution of NaOH (1.8 g, 45 mmol) in water (10 mL) was slowly added. The mixture was refluxed for 2 h. 25 mL of ethanol was added and the mixture was cooled to temperature slowly and dark yellow solid precipitated. The product was isolated by filtration and washed with cold ethanol, with a yield of 47%. Elemental analysis calcd. for $C_{12}H_7NNa_2O_5$ (%): C, 49.50; H, 2.42; N, 4.81. Found(%): C, 49.41; H, 2.67; N, 4.79. FTIR (KBr, cm^{-1}): 3 348, 1 615, 1 507, 1 480, 1 421, 1 385, 1 315, 1 265, 1 107, 948, 824.

1.2.2 Synthesis of $[MnL(H_2O)_3]\cdot H_2O$ (**1**)

To an aqueous solution (5 mL) of $MnCl_2\cdot 4H_2O$ (0.2 mmol, 39.6 mg) was added a methanol solution (15 mL) of Na_2L (0.2 mmol, 58.2 mg). The resulting mixture was stirred for 3 h at room temperature. After filtration, yellow prism crystals suitable for X-ray diffraction were obtained by slow evaporation of the filtrate after ten days, which were collected by filtration, washed with diethyl ether and dried in air (Yield: 28%). Elemental analysis calcd. for $C_{12}H_7MnNO_9$ (%): C, 39.58; H, 1.94; N, 3.85. Found (%): C, 39.49; H, 2.01; N, 3.78. FTIR (KBr, cm^{-1}): 3 333, 1 634, 1 506, 1 480, 1 420, 1 380, 1 318, 1 262, 1 108, 946, 924, 821, 614.

1.2.3 Synthesis of $[CoL(H_2O)_3]\cdot H_2O$ (**2**)

Complex **2** was prepared using a similar procedure with the case of **1**, using $Co(NO_3)_2\cdot 6H_2O$ instead of adding $MnCl_2\cdot 4H_2O$ to the reaction mixture. Red prism crystals suitable for X-ray diffraction were precipitated by slow evaporation of the filtrate after seven days, which were collected by filtration, washed with cold diethyl ether and dried in vacuum (Yield: 37%). Elemental analysis calcd. for $C_{12}H_7CoNO_9$ (%): C, 39.15; H, 1.92; N, 3.80. Found (%): C, 39.08; H, 1.99; N, 3.62. FTIR (KBr, cm^{-1}): 3 381, 1 624, 1 509, 1 480, 1 423, 1 383, 1 316, 1 266, 1 110, 948, 884, 822, 697.

1.3 X-ray crystallography

Single crystals of the complexes with suitable size (0.20 mm×0.10 mm×0.05 mm for **1** and 0.25 mm×0.20 mm×0.10 mm for **2**) were selected. X-ray diffraction data were collected on a Bruker Smart 1000 CCD diffractometer using Mo $K\alpha$ radiation (λ= 0.071 073 nm) with the ω-2θ scan technique. Diffraction data were collected at 113(2) and 293(2) K for **1** and **2**, respectively. All the crystal structures were solved using direct methods (SHELXS-97)[20] and refined with full-matrix least-squares technique on F^2 using the SHELXL-97[21]. The hydrogen atoms were added theoretically, and riding on the concerned atoms and refined with fixed thermal factors. Crystallographic data details and structure refinement parameters are presented in Table 1. Selected bond lengths and angles are listed in Table S1.

CCDC: 1040326, **1**; 1040325, **2**.

1.4 DNA-binding and cleavage experiments

DNA-binding and cleavage experiments were conducted using the similar methods described previously[22-24]. Electronic absorption spectroscopy was an effective method in examining the binding mode of DNA with the metal complex[25]. Specifically,

Table 1 Crystallographic data for complexes 1 and 2

Complex	1	2
Empirical formula	$C_{12}H_{15}MnNO_9$	$C_{12}H_{15}CoNO_9$
Formula weight	372.19	376.18
Crystal system	Triclinic	Triclinic
Space group	$P\bar{1}$	$P\bar{1}$
a / nm	0.738 3(7)	0.729 10(15)
b / nm	0.818 5(8)	0.824 00(16)
c / nm	1.213 1(11)	1.198 9(2)
α / (°)	85.45(3)	84.96(3)
β / (°)	80.04(3)	80.38(3)
γ / (°)	84.36(3)	84.63(3)
V / nm^3	0.717 1(12)	0.705 1(2)
Z	2	2
D_c / (g·cm^{-3})	1.724	1.772
F(000)	382	386
θ range for data collection / (°)	2.81~25.01	3.08~25.01
Limiting indices, hkl	$-8 \leqslant h \leqslant 8, -9 \leqslant k \leqslant 9, -14 \leqslant l \leqslant 14$	$-8 \leqslant h \leqslant 8, -9 \leqslant k \leqslant 9, -13 \leqslant l \leqslant 14$
Reflections collected	4 565	4 052
Independent reflections	2 540 (R_{int}=0.051 3)	2 490 (R_{int}=0.070 8)
Goodness-of-fit on F^2	1.115	1.035
R_1, wR_2 [$I>2\sigma(I)$]	0.111 6, 0.272 3	0.087 8, 0.187 0
R_1, wR_2 (all data)	0.115 1, 0.274 3	0.136 6, 0.212 4
Largest diff. peak and hole / (e·nm^{-3})	2 266 and −601	850 and −714

concentration of CT-DNA was measured from the UV absorption intensity at 260 nm with a molar extinction coefficient of 6 600 L·mol^{-1}·cm^{-1} [26]. The DNA was demonstrated sufficiently free of protein as a ratio of 1.8~1.9 was obtained for the absorbance at 260 nm and 280 nm of the CT-DNA solution, which was carried out in 5 mmol·L^{-1} Tris-HCl/50 mmol·L^{-1} NaCl buffer (pH=7.2)[25]. The absorption spectra of the complexes binding to DNA were performed by increasing addition of CT-DNA to the complexes in Tris-HCl buffer (pH=7.2).

The fluorescence spectra were recorded at room temperature with excitation at 510 nm and emission at about 602 nm. The relative binding of complexes to CT-DNA were carried out with an EB-bound CT-DNA solution in 5 mmol·L^{-1} Tris-HCl and 50 mmol·L^{-1} NaCl buffer (pH=7.2). Absorption titration experiments were performed by titrating complexes into EB-DNA solution, which contains 2.4×10^{-6} mol·L^{-1} EB and 4.8×10^{-5} mol·L^{-1} CT-DNA.

To explore the DNA cleavage abilities of complexes, the supercoiled (SC) pBR322 plasmid DNA as a substrate was incubated with complexes. The DNA cleavage experiments were performed by agarose gel electrophoresis, Details of the measurement was carried out as follows: A solution of pBR322 DNA (0.1 μg·μL^{-1}) in Tris-HCl (50 mmol·L^{-1}) and NaCl (18 mmol·L^{-1}) buffer (pH=7.2) was treated with **1** and **2**. After incubation at 37 ℃ for 3 h, the buffer of bromophenol blue (0.25%), glycerol (45%) and EDTA (2 mmol·L^{-1})) was added. The samples were electrophoresed at 120 V on 0.9% agarose gel for 2 h, using Tris-boric acid-EDTA buffer. The extent of cleavage of the super coiled DNA (SC DNA) was determined by measuring the intensities of the bands, which were visualized by UV light and photographed using the Gel Documentation System[27].

Cleavage mechanistic of pBR322 DNA was investigated in the presence of reaction inhibitors and standard radical scavengers. KI, NaN_3, methyl green,

SYBR green, EDTA and SOD were used as standard radical scavengers, which were added to pBR322 DNA prior to complex loading. After the addition of complex, cleavage experiment was initiated, and it was quenched with addition of 2 μL buffer. Further analysis was carried out using the above standard method.

1.5 Protein binding studies

The protein binding study was conducted with tryptophan fluorescence quenching experiments using BSA stock solution (1.5 mmol·L^{-1}) in 10 mmol·L^{-1} phosphate buffer (pH=7.0)[23]. Briefly, a similar stock solution was prepared as the DNA binding experiments, except that phosphate buffer was used instead of Tris-HCl buffer. Fluorescence spectra were recorded at room temperature with excitation wavelength of BSA at 280 nm and emission at 342 nm. The concentration of BSA was kept constant (36.6 μmol·L^{-1}) while the complex concentration varying from 0 to 6.39 μmol·L^{-1}. Absorption titration experiments with BSA (15 μmol·L^{-1}) were carried out in the absence and presence of complex (2 μmol·L^{-1}) (pH=7.0).

2 Results and discussion

2.1 Description of the crystal structures

Mononuclear complexes **1** and **2** have been structurally characterized by X-ray crystallography. Since the two complexes are isostructural, the molecular structure of **1** was shown representatively in Fig.1 (A similar structure of **2** was shown as Fig.S1). Parameters of refinement process and selected bond lengths and angles are listed in Table 1 and S1, respectively.

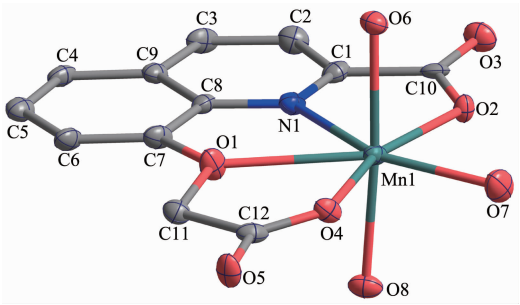

Hydrogen atoms and dissociative small molecule are omitted for clarity

Fig.1 ORTEP view of the molecular structure and atom-labeling scheme of complex **1** with 30% probability ellipsoid

The complexes are isostructural and crystallize in a triclinic cell with $P\bar{1}$ space group. Both metal centers are hepta-coordinated with O_6N donor sets and the geometry around metal centers can be best described as distorted pentagonal bipyramidal. It is worth mentioning that weak M-O(1) coordinated interactions (Mn(1)-O(1) 0.249 7(10) nm, Co(1)-O(1) 0.251 4(7) nm) exist in the [ML$(H_2O)_3$] units, which are supposed to be caused by the rigid structure of 8-hydroxy-2-methylquinoline[19]. The nitrogen atom (N(1)), three oxygen atoms (O(1), O(2) and O(4)) of the ligand and an oxygen atom (O(7)) of coordinate water molecule form the basal plane. Another two oxygen atoms (O(6) and O(8)) of water molecule occupy the axial positions with normal M-O bond distances, and the trans-axial angles(O6-M-O8) are 176.8(4)° for **1** and 174.9(3)° for **2**, respectively. The angles (Table S1) around the metal ion within the pentagonal basal plane vary from 64.3(4)° to 81.4(4)° for complex **1** (64.0(2)°~80.7(3)° for complex **2**), and the sum of angles spanning these five bonds is 360° for complex **1** (360.2° for complex **2**), underscoring the flat nature of this equatorial plane.

2.2 DNA-binding and cleavage activities

2.2.1 DNA-binding studies

The interaction of complexes with CT-DNA was monitored by absorption spectral titrations. The typical titration curve as well as a plot of $(\varepsilon_a-\varepsilon_f)/(\varepsilon_b-\varepsilon_f)$ versus c_{DNA} for the titration of DNA to complex **2** is shown in Fig.2 (similar spectrum of **1** is provided as Fig.S2). The observed intense absorption peaks at 217~221 nm for the two complexes are assigned to the π-π^* transition of intraligand. Addition of increasing amounts of CT-DNA results in an appreciable hypochromism of complexes and slight red shifts (3 nm) in band position, which indicates partial intercalation between complexes and DNA[28]. Due to the strong stacking interaction between an aromatic chromophore and the base pairs of DNA, the intercalation between complexes and DNA would lead to hypochromism or bathochromism in UV absorption

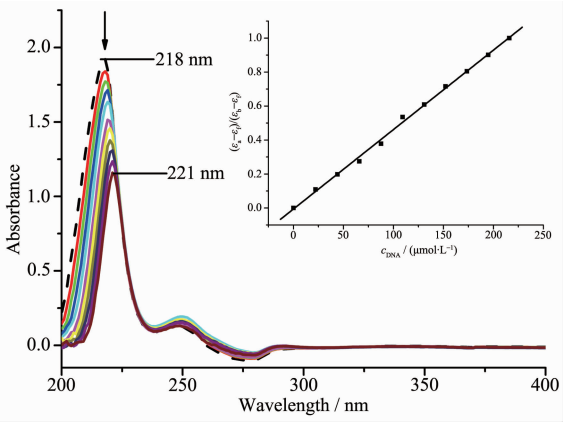

From top to bottom: c_{DNA}=22.1, 44.0, 65.9, 87.6, 109.3, 130.8, 152.3, 173.6, 194.8 and 216.0 μmol·L^{-1}, respectively; Inset: plot of $(\varepsilon_a-\varepsilon_f)/(\varepsilon_b-\varepsilon_f)$ versus c_{DNA} for the titration of DNA to complex

Fig.2　Absorption spectra of complex **2** (2.5 μmol·L^{-1}, 0.015% DMF/H_2O) in the absence (dashed line) and presence (solid line) of increasing amounts of CT-DNA in 5 mmol·L^{-1} Tris-HCl/50 mmol·L^{-1} NaCl buffer (pH=7.2)

spectra. In order to determine the binding strength of the complexes with CT-DNA, the intrinsic binding constants K_b for complexes **1** and **2** were determined from the spectral titration according to the following equation[29]: $c_{DNA}/(\varepsilon_a-\varepsilon_f)=c_{DNA}/(\varepsilon_b-\varepsilon_f)+1/[K_b(\varepsilon_b-\varepsilon_f)]$, where c_{DNA} is the DNA concentration in nucleotides. The apparent absorption coefficient ε_a, ε_b and ε_f correspond to the extinction coefficient observed for the charge transfer absorption band at a given DNA concentration, the complex free in solution, the complex when fully bound to DNA, respectively. The binding constant K_b values (Table 2) follow the order: **2** (7.45×10^5 L·mol^{-1}) > **1** (4.09×10^5 L·mol^{-1}), which suggest that complex **2** has stronger binding affinity than **1**.

As a means for better understanding of the interaction of the compound with DNA, fluorescence spectral measurements were performed on CT-DNA by varying the concentration of the complexes. Since no luminescence is observed for both complexes at room temperature, ethidium bromide (EB) was employed as fluorescence probe and the binding propensity of the complexes to CT-DNA is evaluated by fluorescence emission intensity of EB bound to DNA. Due to the strong intercalation to the adjacent DNA base pairs, EB could emit intense fluorescent light in the presence of DNA[30] and could be quenched by addition of another molecule. Fig.3(a) shows the relative

Table 2　DNA and BSA binding data for complexes 1 and 2

Complex	Complex / CT-DNA		Complex / BSA			
	K_b / (L·mol^{-1})	K_{app} / (L·mol^{-1})	K_{SV} / (L·mol^{-1})	K_q / (L·mol^{-1}·s^{-1})	K / (L·mol^{-1})	n
1	4.09×10^5	4.16×10^5	2.46×10^4	2.46×10^{12}	3.67×10^3	0.84
2	7.45×10^5	6.76×10^5	1.58×10^4	1.58×10^{12}	48.2	0.52

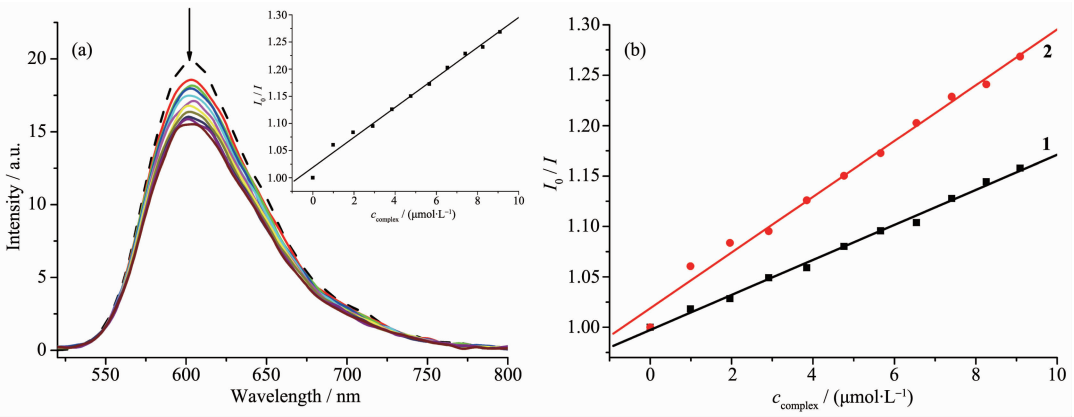

From top to bottom: $c_{complex}$=0.99, 1.96, 2.91, 3.85, 4.76, 5.66, 6.54, 7.41, 8.26 and 9.09 μmol·L^{-1}, respectively; Inset in (a): plot of I_0/I versus concentration of the complex

Fig.3　(a) Fluorescence emission spectra of the EB (2.4 μmol·L^{-1}) bound to CT-DNA (48 μmol·L^{-1}) system in the absence (dashed line) and presence (solid lines) of complex **2**; (b) Plots of I_0/I versus the concentrations of complexes **1** and **2**

binding propensity of the complex **2** to EB bound CT-DNA and similar spectrum of **1** is presented as Fig. S3. Plots of I_0/I versus $c_{complex}$ for the quenched intensity of **1**~**2** to EB-DNA is shown in Fig.3(b). The reduction extent of the emission intensity at 602 nm (510 nm excitation) provides an evaluation of the binding propensity of the complex to DNA. On the basis of the Stern-Volmer equation[31], $I_0/I=1+Kc_Q$, in which I_0 and I represent the fluorescence intensities in the absence and presence of quencher, K is the Stern-Volmer quenching constant, and c_Q is the concentration of the quencher, the quenching plots showed that the quenching of EB bound to CT-DNA by complex **1** or **2** is in agreement with the linear Stern-Volmer equation, which also indicates that the complexes performed good bind ability to DNA. According to equation $K_{EB}c_{EB}=K_{app}c_{complex}$, where the $c_{complex}$ was the concentration value at half reduction of the fluorescence intensity of EB, and K_{EB} was a constant of 1.0×10^7 mol·L^{-1} (c_{EB}=2.4 μmol·L^{-1}). The calculated apparent binding constant values (K_{app}) (Table 2) follow the order: **2** (6.76×10^5 L·mol^{-1}) > **1** (4.16×10^5 L·mol^{-1}), which is consistent with the results of K_b values by UV spectroscopy. The two complexes show better binding propensity than the previous reported Co(Ⅱ) and Mn(Ⅱ) complexes[32-34]. On the whole, the binding constants are less than that of the classical intercalators and metallointercalators (10^7 L·mol^{-1})[35], indicating medium binding strength of the complexes with CT-DNA.

2.2.2 DNA cleavage studies

The concentration-dependent DNA cleavage activity by complex **2** was observed without any external agents, as shown in Fig.4(a) (similar study of **1** is presented as Fig.S4(a)). **2** could not induce obvious DNA cleavage with the increase of concentration (50~650 μmol·L^{-1}), while the percentages of Form Ⅰ (SC DNA) and Form Ⅱ (NC DNA) of complex **1** both gradually reduce with the increase of concentration, which suggests that the complex partially degraded SC DNA into undetectable minor fragments[36].

The concentration-dependent DNA cleavage activities by complex **1** and **2** were also performed in the presence of reductive reagent H_2O_2. The results showed that DNA cleavage efficiency of complex **2** exhibited remarkable increases at the same conditions (Fig.4(b)). It has been observed that complex **2** is an efficient cleaver of SC DNA and produces ~93% of NC DNA at 20 μmol·L^{-1} concentration, which implies that H_2O_2 plays a vital role as a revulsant or an activator. While **1** shows relatively weak chemical nuclease activity which implies little impact on the reductive reagent. As shown in the Fig.S4(b) and Fig. 4(b), at 50 μmol·L^{-1} concentration, the DNA cleavage efficiencies (Form Ⅰ into Form Ⅱ and Form Ⅲ) follow the order of **2** (90.3% Form Ⅱ and 9.7% Form Ⅲ)>**1** (47.5% Form Ⅱ).

In order to get further information about the reactive oxygen species (ROS) which was responsible for the DNA damage, the potential DNA cleavage mechanism of the complexes in the presence of H_2O_2 were investigated. Series of DNA cleavage experiments (Fig.5 and Fig.S5) were performed using additional reagents like KI as hydroxyl radical (OH·) scavengers, NaN_3 as singlet oxygen ($^1O_2$) quencher, methyl green as DNA major groove-binder, SYBR green as DNA minor groove-binder, EDTA as the chelator of complexes and superoxide dismutase (SOD) as O_2^-· radical scavenger. As Fig.5 shows, the complexes showed complete or partial inhibition in the DNA-cleavage

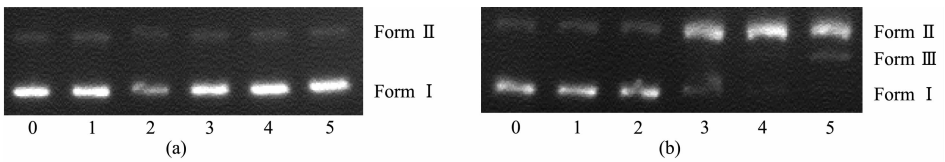

(a) Lane 0: DNA control (3 h), Lane 1~5: DNA+complex **2** (50, 200, 350, 500, 650 μmol·L^{-1}); (b) Lane 0: DNA control (3 h); Lane 1: DNA+0.25 m mol·L^{-1} H_2O_2; Lane 2~5: DNA+H_2O_2+complex **2** (5, 20, 35, 50 μmol·L^{-1})

Fig.4 Gel electrophoresis diagram showing the cleavage of pBR322 DNA (0.1 μg·μL^{-1}) at different complex concentrations in Tris-HCl/NaCl buffer (pH=7.2) and 37 ℃

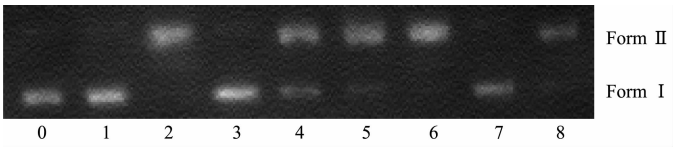

Lane 0: DNA control; Lane 1: DNA+0.25 mmol·L^{-1} H_2O_2; Lane 2: DNA+0.25 mmol·L^{-1} H_2O_2+complex 2; Lane 3~8: DNA+0.25 mmol·L^{-1} H_2O_2+ complex **2**+inhibitors (0.01 mol·L^{-1} KI, 0.01 mol·L^{-1} NaN_3, 0.1 mmol·L^{-1} methyl green, 0.15 μL·mL^{-1} SYBR green, 0.5 mmol·L^{-1} EDTA, 2 U·mL^{-1} SOD, respectively)

Fig.5　Cleavage of plasmid pBR322 DNA (0.1 μg·μL^{-1}) in presence of 35 μmol·L^{-1} complex **2** (0.1% DMF/H_2O) and different inhibitors after 3 h incubation at 37 ℃

activity in the presence of the hydroxyl radial scavenger KI, no obvious inhibitions were observed for other radical scavengers (Fig.6), which suggested the involvement of hydroxyl radicals (OH·) as reactive oxygen species. The EDTA, a metal chelating agent that strongly binds to M(Ⅱ) forming a stable complex, can efficiently inhibit DNA cleavage, indicating the metal ion play the key role in the cleavage. Moreover, the additions of DNA major groove-binder methyl green and minor groove-binder SYBR Green showed no inhibition DNA cleavage by complexes **1** and **2**, which suggested that the complexes didn't bind at the grooves of DNA[37].

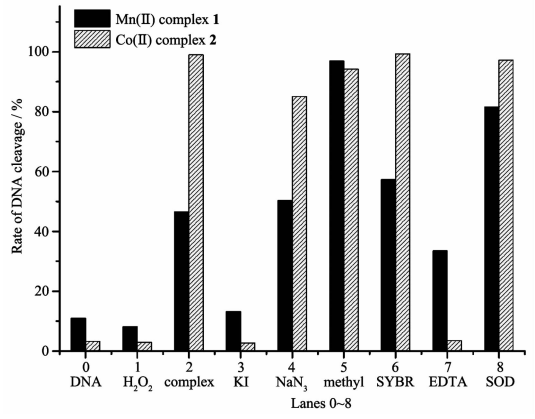

c_1=50 μmol·L^{-1}, c_2=35 μmol·L^{-1}

Fig.6　Histogram of relative amounts according to Fig.S5 and Fig.5 shows the cleavage of plasmid pBR322 DNA (0.1 μg·μL^{-1}) in presence of complex and different inhibitors after 3 h incubation at 37 ℃

2.3　Protein binding studies

The interactions between drugs with blood plasma proteins have attracted increasing research interest in recent years, particularly regarding serum albumin. Since serum albumin constitutes more than half of the total protein in blood plasma and it plays an important role in drug transport and drug metabolism[37-38], and may lead to enhancement of the biological properties of the original drug[39]. Bovine serum albumin (BSA) is extensively studied for its structural homology with human serum albumin (HSA). The fluorescence property of BSA is due to the presence of tryptophan, tyrosine and phenylalanine residues, and tryptophan is the most primary contributor[38]. Fig.7(a) shows the fluorescence emission spectrum of BSA with increasing concentration of complex **1** (similar spectrum of **2** is presented as Fig. S6). When complexes concentration was increased, the intensity of the characteristic broad emission band at 348 nm decreased regularly, which demonstrate that the interactions between complexes and BSA have indeed occurred. The fluorescence quenching can be described according to Stern-Volmer equation, $F_0/F = 1+K_q\tau_0 c_Q = 1+K_{SV}c_Q$. F_0 and F respectively represent the fluorescence intensities in the absence and presence of quencher, K_q represents the quenching rate constant, τ_0 is the average life-time of biomolecule without quencher (about 10^{-8} s)[31], K_{SV} is the Stern-Volmer quenching constant and c_Q represents the quencher concentration. Fig.7(b) shows the Stern-Volmer plots of F_0/F vs c_Q of the complexes, and K_{SV} can be obtained by the slope from the plot. Table 2 listed the values of K_{SV} and K_q for the interaction of the complexes with BSA and the K_{SV} values follow the order: **1** (2.46×10^4 mol·L^{-1}) > **2** (1.58×10^4 mol·L^{-1}).

In general, quenching mechanisms can be classified as dynamic and static quenching. Dynamic quenching takes a process of interaction between the fluorophore and the quencher during the transient

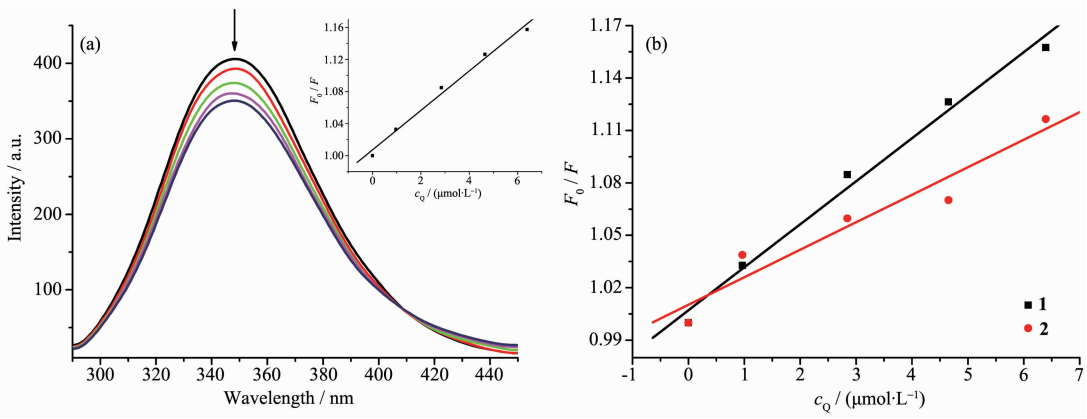

From top to bottom: $c_{complex}$=0.97, 2.84, 4.65 and 6.39 μmol·L^{-1}, respectively; Inset in (a): plot of F_0/F versus the complex concentration

Fig.7 (a) Fluorescence emission spectra of the BSA (36.6 μmol·L^{-1}) system in the absence (dashed line) and presence (solid lines) of complex **1**; (b) Plot of F_0/F versus the concentration of complexes **1** and **2**

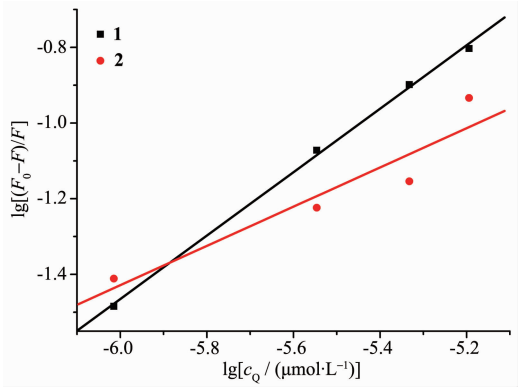

Fig.8 Plot of lg[(F_0–F)/F] vs lgc_Q for BSA in the presence of complexes **1** and **2**

existence of the exited state while static quenching tends to the formation of fluorophore-quencher complex. The K_q values (~10^{12} L·mol^{-1}·s^{-1}) of **1** and **2** are higher than the maximum scatter collision-quenching constant of diverse kinds of quenchers for biopolymers fluorescence (2×10^{10} L·mol^{-1}·s^{-1}, the maximum possible value for dynamic quenching), suggesting the presence of static quenching mechanism[40].

On the basis of the Scatchard equation[41]: lg[(F_0–F)/F]=lg$K$+$n$lgc_Q, for the static quenching interaction, the binding constant (K) and the number of binding sites (n) can be respectively calculated from the slope and the intercept of the double logarithm regression plots of lg[(F_0–F)/F] versus lgc_Q (Fig.8). Table 2 shows the K and n values following the order: **1** (3.67×10^3 L·mol^{-1}, 0.84)> **2** (48.2 L·mol^{-1}, 0.52), indicating that **1** exhibits higher binding constants for BSA than **2**, which is inconsistent with the results of DNA interaction. As expected, the values of n are associated with binding constants K, which verify the conclusion [42] that a direct relation between the binding constant and number of binding sites.

UV-Vis absorption spectroscopy, which is a simple but effective method for detecting complex formation, was employed to detect changes of the intensity and wavelength of complex with BSA. The absorption band obtained in the spectra of 15 μmol·L^{-1} BSA at 279 nm in the absence of complex, and the intensity showed an increase without any shift after the addition of 2 μmol·L^{-1} Mn(Ⅱ) and Co(Ⅱ) complexes, respectively (Fig.9), which can be attributed to the formation of a ground state complex between metal complex and BSA[43]. Mn(Ⅱ) complex showed a larger hyperchromism of 3.6% than that of Co(Ⅱ) complexes (0.9%), indicating that Mn(Ⅱ) behaved stronger ability of BSA binding, which was consistent

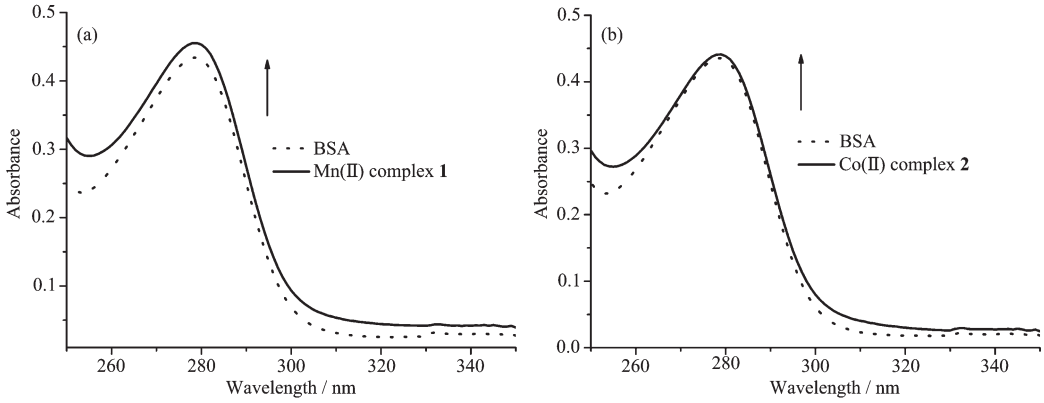

Fig.9　Absorption spectra of BSA (15 μmol·L^{-1}) in the absence (dot line) and presence (solid line) of complexes **1** (a) and **2** (b) (2 μmol·L^{-1}) in phosphate buffer (pH=7.0)

with the results of fluorescence tests.

3　Conclusions

Two new mononuclear Mn(Ⅱ) and Co(Ⅱ) complexes have been synthesized and characterized by using various physico-chemical techniques. Crystal structures of the complexes are isostructural and both metal centers are hepta-coordinated and the geometry can be described as distorted pentagonal bipyramidal. The complexes display binding propensity to the CT-DNA giving a relative order: **2** (Co(Ⅱ) complex)> **1** (Mn(Ⅱ) complex). Compared with complex **1**, the DNA cleavage efficiency of **2** exhibited more remarkable increases at the same condition in the presence of H_2O_2. Oxidative mechanism has been demonstrated by adding standard radical scavengers and the reactive oxygen species (ROS) responsible for the DNA cleavage is likely hydroxyl radicals (OH·). While binding abilities of the complexes to BSA are inconsistent with the results of DNA interaction which follow the order: **1**>**2**, and the quenching mechanisms of BSA by the complexes are static procedures.

Acknowledgements: This work was supported by the PhD Research Startup Foundation of Shanxi Agricultural University (Grants No.2013YJ40 and 2013YJ41), Science and Technology Innovation Fund of Shanxi Agricultural University (Grants No.2014005 and 2014013), College students Innovation and Entreprenecuship Training Project of Shanxi province (Grants No.2015085 and 2015/06) and the Key Scientific Research Projects of Coal Fund in Shanxi (Grant No.FT201402-01).

Supporting information is available at http://www.wjhxxb.cn

References:

[1] Barone G, Terenzi A, Lauria A, et al. *Coord. Chem. Rev.*, **2013**,**257**(19):2848-2862

[2] Jiang Q, Xiao N, Shi P, et al. *Coord. Chem. Rev.*, **2007**,**251**(15):1951-1972

[3] Pages B J, Ang D L, Wright E P, et al. *Dalton Trans.*, **2015**, **44**(8):3505-3526

[4] Rosenberg B, Van Camp L, Krigas T. *Nature*, **1965**,**205**:698-699

[5] Rosenberg B, Van camp L. *Nature*, **1969**,**222**:385-386

[6] Mjos K D, Orvig C. *Chem. Rev.*, **2014**,**114**(8):4540-4563

[7] Wilson J J, Lippard S J. *Chem. Rev.*, **2013**,**114** (8):4470-4495

[8] Storr T, Thompson K H, Orvig C. *Chem. Soc. Rev.*, **2006**,**35** (6):534-544

[9] Reedijk J. *Proc. Natl. Acad. Sci. U.S.A.*, **2003**,**100**(7):3611-3616

[10]Komor A C, Barton J K. *Chem. Commun.*, **2013**,**49**(35):3617-3630

[11]Leung C H, He H Z, Liu L J, et al. *Coord. Chem. Rev.*, **2013**,**257**(21):3139-3151

[12]Liu H K, Sadler P J. *Acc. Chem. Res.*, **2011**,**44**(5):349-359

[13]Aiba Y, Sumaoka J, Komiyama M. *Chem. Soc. Rev.*, **2011**, **40**(12):5657-5668

[14]Munteanu C R, Suntharalingam K. *Dalton Trans.*, **2015**,**44** (31):13796-13808

[15]Ghosh K, Tyagi N, Kumar P. *Inorg. Chem. Commun.*, **2010**, **13**(3):380-383

[16]Ghosh K, Mohan V, Kumar P, et al. *Polyhedron*, **2013**,**49**(1): 167-176

[17]Daniel K G, Chen D, Orlu S, et al. *Breast Cancer Res.*,

2005,**7**(6):R897-R908

[18]Chen D, Peng F, Cui Q C, et al. *Front. Biosci.*, **2005**,**10**(2):2932-2939

[19]Zheng Q, Wang S, Liu W. *Tetrahedron*, **2014**,**70**(42):7686-7690

[20]Sheldrick G M. *SHELXS*-97, *Program for the Solution of Crystal Structure*, University of Göttingen, Germany, **1997**.

[21]Sheldrick G M. *SHELXL*-97, *Program for the Refinement of Crystal Structure*, University of Göttingen, Germany, **1997**.

[22]Gao C Y, Ma Z Y, Zhang Y P, et al. *RSC Adv.*, **2015**,**5**(39):30768-30779

[23]Gao C Y, Qiao X, Ma Z Y, et al. *Dalton Trans.*, **2012**,**41**(39):12220-12232

[24]Zhang Y P, Ma Z Y, Gao C Y, et al. *New J. Chem.*, **2016**,**40**(9):7513-7521

[25]Marmur J. *J. Mol. Biol.*, **1961**,**3**(2):208-218

[26]Gultneh Y, Khan A R, Blaise D, et al. *J. Inorg. Biochem.*, **1999**,**75**(1):7-18

[27]Bernadou J, Pratviel G, Bennis F, et al. *Biochemistry*, **1989**, **28**(18):7268-7275

[28]Baldini M, Belicchi-Ferrari M, Bisceglie F, et al. *Inorg. Chem.*, **2004**,**43**(22):7170-7179

[29]Wolfe A, Shimer Jr G H, Meehan T. *Biochemistry*, **1987**,**26**(20):6392-6396

[30]Meyer-Almes F J, Porschke D. *Biochemistry*, **1993**,**32**(16):4246-4253

[31]Lakowicz J R, Weber G. *Biochemistry*, **1973**,**12**(21):4171-4179

[32]Ramachandran E, Thomas S P, Poornima P, et al. *Eur. J. Med. Chem.*, **2012**,**50**:405-415

[33]Kellett A, O′Connor M, McCann M, et al. *MedChemComm*, **2011**,**2**(7):579-584

[34]Wu H, Shi F, Wang X, et al. *Transition Met. Chem.*, **2014**, **39**(3):261-270

[35]Cory M, McKee D D, Kagan J, et al. *J. Am. Chem. Soc.*, **1985**,**107**(8):2528-2536

[36]Ramakrishnan S, Shakthipriya D, Suresh E, et al. *Inorg. Chem.*, **2011**,**50**(14):6458-6471

[37]Gibellini D, Vitone F, Schiavone P, et al. *J. Clin. Virol.*, **2004**,**29**(4):282-289

[38]Lakowicz J R. *Principles of Fluorescence Spectroscopy*. 3*rd Ed*. New York: Springer, **2006**:530-573

[39]Villarreal W, Colina-Vegas L, Rodrigues de Oliveira C, et al. *Inorg. Chem.*, **2015**,**54**(24):11709-11720

[40]Ware W R. *J. Phys. Chem.*, **1962**,**66**(3):455-458

[41]Scatchard G. *Ann. N. Y. Acad. Sci.*, **1949**,**51**(4):660-672

[42]Sathyadevi P, Krishnamoorthy P, Butorac R R, et al. *Dalton Trans.*, **2011**,**40**(38):9690-9702

[43]Hu Y J, Ou-Yang Y, Dai C M, et al. *Biomacromolecules*, **2009**,**11**(1):106-112